

Contents lists available at ScienceDirect

Petroleum Science

journal homepage: www.keaipublishing.com/en/journals/petroleum-science



Original Paper

Performance and enhanced oil recovery efficiency of an acid-resistant polymer microspheres of anti-CO₂ channeling in low-permeability reservoirs



Hai-Zhuang Jiang ^{a, c}, Hong-Bin Yang ^{a, c, *}, Ruo-Sheng Pan ^b, Zhen-Yu Ren ^b, Wan-Li Kang ^{a, c, d}, Jun-Yi Zhang ^{a, c}, Shi-Long Pan ^{a, c}, Bauyrzhan Sarsenbekuly ^{a, d}

- ^a State Key Laboratory of Deep Oil and Gas, China University of Petroleum (East China), Qingdao, 266580, Shandong, PR China
- ^b Oil and Gas Engineering Research Institute, CNPC Jilin Oilfield Company, Songyuan, 138000, Jilin, PR China
- ^c School of Petroleum Engineering, China University of Petroleum (East China), Qingdao, 266580, Shandong, PR China
- ^d School of Energy and Petroleum Industry, Kazakh-British Technical University, Almaty, 050000, Kazakhstan

ARTICLE INFO

Article history: Received 20 July 2023 Received in revised form 1 February 2024 Accepted 2 February 2024 Available online 4 February 2024

Edited by Yan-Hua Sun

Keywords: Low-permeability reservoir Anti-CO₂ channeling Polymer microsphere Acid resistance

ABSTRACT

CO₂ flooding is a vital development method for enhanced oil recovery in low-permeability reservoirs. However, micro-fractures are developed in low-permeability reservoirs, which are essential oil flow channels but can also cause severe CO₂ gas channeling problems. Therefore, anti-gas channeling is a necessary measure to improve the effect of CO2 flooding. The kind of anti-gas channeling refers to the plugging of fractures in the deep formation to prevent CO₂ gas channeling, which is different from the wellbore leakage. Polymer microspheres have the characteristics of controllable deep plugging, which can achieve the profile control of low-permeability fractured reservoirs. In acidic environments with supercritical CO₂, traditional polymer microspheres have poor expandability and plugging properties. Based on previous work, a systematic evaluation of the expansion performance, dispersion rheological properties, stability, deep migration, anti-CO₂ channeling and enhanced oil recovery ability of a novel acid-resistant polymer microsphere (DCNPM-A) was carried out under CQ oilfield conditions (salinity of 85,000 mg/L, 80 °C, pH = 3). The results show that the DCNPM-A microsphere had a better expansion performance than the traditional microsphere, with a swelling rate of 13.5. The microsphere dispersion with a concentration of 0.1%-0.5% had the advantages of low viscosity, high dispersion and good injectability in the low permeability fractured core. In the acidic environment of supercritical CO₂, DCNPM-A microspheres showed excellent stability and could maintain strength for over 60 d with less loss. In core experiments, DCNPM-A microspheres exhibited delayed swelling characteristics and could effectively plug deep formations. With a plugging rate of 95%, the subsequent enhanced oil recovery of CO₂ flooding could reach 21.03%. The experimental results can provide a theoretical basis for anti-CO₂ channeling and enhanced oil recovery in low-permeability fractured reservoirs.

© 2024 The Authors. Publishing services by Elsevier B.V. on behalf of KeAi Communications Co. Ltd. This is an open access article under the CC BY-NC-ND license (http://creativecommons.org/licenses/by-nc-nd/4.0/).

1. Introduction

Recently, there has been an increasing focus on carbon capture and sequestration. Some oilfields or oilfield service companies are gradually moving towards to carbon capture, utilization and sequestration (CCUS) (Liu et al., 2022; Ren et al., 2022; Suicmez,

2019). Some oilfields in China (Changqing, Yanchang, Shengli, Jilin, etc.) use CO_2 to enhance oil recovery (EOR) to achieve "carbon utilization", and these oilfields all have low-permeability characteristics (Li et al., 2014, 2018; Lv et al., 2021a; Ren et al., 2016). CO_2 has the advantages of low mobility, similar polarity with crude oil, expandable crude oil and easy mixing, which have been considered in the development of low-permeability oilfields (Kang et al., 2021). Furthermore, due to the poor physical properties of the low-permeability reservoir, CO_2 flooding has more significant advantages than water flooding. Artificial fracturing is often used to

^{*} Corresponding author. State Key Laboratory of Deep Oil and Gas, China University of Petroleum (East China), Qingdao, 266580, Shandong, PR China *E-mail address*: hongbinyang@upc.edu.cn (H.-B. Yang).

increase the oil drainage area in low-permeability reservoirs, which leads to the problem of gas channeling when CO₂ flooding is used, resulting in serious effects on oil field development. Therefore, the problem of anti-gas channeling in low-permeability fractured reservoirs flooded with CO₂ has existed for a long time (He et al., 2015).

The reservoir formation is acidic due to the long-term CO₂ oil displacement. To prevent CO₂ gas channeling, many scholars have proposed several methods, including water-alternating-gas injection (WAG), CO₂ thickening, CO₂ foam, polymer gel, polymer gel particles (microspheres), etc. (Guzmán-Lucero et al., 2022; Pal et al., 2022; Rahmani, 2018; Ren and Duncan, 2021; Paul and Bai, 2015; Yang et al., 2023b). Some studies of anti-CO₂ gas channeling in lowpermeability reservoirs in the last three years are listed in Table 1. Among them, the cost of the auxiliary agent (siloxane-type polymer, fluorine surfactant) used for CO2 thickening is high and its application is limited. The cost problem also exists for the CO₂responsive wormlike micelles. WAG, CO2 foam, polymer gel and polymer gel particles are mainly used, which has excellent plugging performance and enhanced oil recovery effect in laboratory research. However, some serious problems have arisen in the practical application of these plugging agents. For example, the long-term stability of CO₂ foam is poor (the fracture cannot provide the porous medium to generate bubble). The short-term WAG shows some effect but the long-term EOR is poor. And the near-well plugging strength of polymer gel is too high to plug the fracture of the far-well. In recent years, polymer gel particles have shown great promise for immiscible CO₂ plugging in the far well zone of fractured reservoirs due to their advantages of controllable particle size, deep migration, accumulation and plugging (Zou et al., 2018).

In low-permeability oilfields where CO_2 flooding is used, the pressure and temperature near the injection well are usually higher than the CO_2 miscible flooding conditions (Ji et al., 2023). Therefore, the problem of CO_2 gas channeling often occurs in the far-well zone,

which requires the plugging agent to have the characteristics of "easy injection, far migration, strong plugging and stable resistance". Polymer gel particles (microspheres) can meet the requirements of anti-CO₂ channeling in low-permeability fractured reservoirs (Amir et al., 2022; Elsharafi and Bai, 2016, 2017; Yang et al., 2023a). In terms of the characteristics of the lowpermeability micro/nano-pore throat, the nano-polymer microspheres (particles) stand out in the anti-CO₂ gas channeling due to its characteristics of controllable particle size, excellent swelling performance (Liu et al., 2020; Zou et al., 2020). During field implementation, the traditional nano-polymer microsphere is limited due to its poor swelling, low plugging strength and poor stability in the acidic reservoir environment of CO₂ flooding. Therefore, the research and development of nano polymer microsphere with acid-resistance is a frontier work for anti-CO₂ channeling, which has the characteristics of "easy injection, far migration, strong plugging and stable acid-resistance" to meet the CO₂ flooding plugging application in acidic reservoir environment.

In the previous research, we developed a novel nano-polymer microsphere (DCNPM-A) with delayed swelling performance, which can meet the characteristics of "easy injection and far migration" (Zhou et al., 2022a). In the molecular structural design, a cationic monomer named diallyl dimethylammonium chloride (DMDAAC) was introduced into the microsphere structure to give the microsphere the advantage of acid-resistance. In this study, we mainly evaluated the performance of nano-polymer microspheres in acidic environments, including swelling performance, injectability, stability and laws of deep migration. Combined with CO₂ flooding and anti-gas channeling experiment, we systematically explored the anti-CO₂ gas channeling performance of the microsphere to meet the characteristics of "easy injection, far migration, strong plugging and stable acid-resistance". It provides theoretical research and technical support for anti-CO₂ gas channeling of nano-

Table 1 Anti CO_2 gas channeling research over the last three years.

Experimental conditions		Type of	Characteristics	Reference	
Temperature, °C	Salinity, mg/L	plugging agent			
40	_	Thickened	The viscosity of supercritical CO ₂ can be increased to 14.87 mPa s with the vinyl polysiloxane thickener.	Zhao et al. (2022)	
80	-	CO ₂	Polydimethylsiloxane-thickened CO ₂ can increase the oil recovery factor by 6%–15% when the core permeability is below $10 \times 10^{-3} \mu m^2$ and the pressure is 21 MPa.	Gandomkar et al. (2021)	
47	_		When the mass concentration of thickener was 5%, the viscosity of CO ₂ was increased by 297 times.	Dai et al. (2022)	
85	-	WAG	The graft copolymer-enhanced WAG processes can increase 21%—22% total oil recovery than the conventional and HAPM-enhanced WAG processes.	Luo et al. (2021)	
70	29,520		Under miscible conditions of 18 MPa, WAG can improve the oil recovery by 16.9% compared with CO ₂ flooding. The oil in the low permeability layer is effectively used.	Wang et al. (2020)	
65	Deionized water	CO ₂ foam	CO_2 foam enhanced oil recovery by 11.4% in the core with permeability of 2.4 μm^2 .	Lv et al. (2021b)	
40	9974.6		CO_2 foam enhanced oil recovery by 18.2%–39.4% when the core permeability contrast ranged from 3.6 to 51.0.	Ding et al. (2022)	
50	Deionized water		The surface-modified silica (SiO_2) reinforced CO_2 foam can improve oil recovery by 15%.	Risal et al. (2019)	
85	80,113.18	Polymer gel	When the core permeability is $1.275 \mu m^2$, the plugging rate of polymer gel was 98.33%.	Zhou et al. (2022b)	
_	Deionized water		For the fractured core with permeability of $81 \times 10^{-3} \mu m^2$, the enhanced oil recovery and plugging rate are 13.3% and 94.62%, respectively.	Canbolat and Parlaktuna (2019)	
45	NaCl with 10,000		The plugging efficiency of polymer gel can reach over 99.99% in the fractured core.	Song et al. (2022)	
_	240,476.6	Polymer gel	The plugging rate of particle was 99.83% when the concentration is 0.5%.	Zhang et al. (2022)	
55	-	particle	Compared with single-layer sandpack, CO ₂ -induced hydrogel can effectively improve the oil recovery of two-layer sandpack.	Nguele et al. (2021)	
68	20,512.59		The plugging efficiency of CO ₂ -responsive preformed gel particles is 99%, and the oil recovery is increased by 23.1%.	Pu et al. (2021)	
50	15,063	Wormlike	Wormlike micelles enhanced oil recovery by 21.7% in the core with 0.25 mm fracture.	Shen et al. (2021)	
90	20,102.4	micelles	Combined CO_2 -responsive gel particle with wormlike micelles, the system enhanced oil recovery by 4% -16% .	Du et al. (2022)	
25	NaCl with 5000		The plugging rate of CO ₂ -switchable wormlike micelles was 99.3%.	Yang Z. et al. (2019)	

polymer microspheres in low-permeability fractured reservoirs.

2. Materials and methods

2.1. Materials and instruments

DCNPM-A microsphere was prepared in the laboratory, and its specific synthesis method was mentioned in a previous study (Zhou et al., 2022a). DCNPM microspheres were prepared by removing the acid-resistant monomer DMDAAC from the synthesis formula of DCNPM-A microspheres. SCNPM-A microspheres were single crosslinking microspheres with acid-resistant monomer DMDAAC. SCNPM microspheres were traditional microspheres without DMDAAC and unstable crosslinking agent. The molecular structures of these four microspheres are shown in Fig. S1. NaCl, CaCl₂, BaCl₂, NaHCO₃ and HCl (analytical grade) were purchased from the Sinopharm Chemical Reagent Co. Ltd. (Shanghai, China). CO₂ (> 99%) was purchased from Qingdao Deyi Gas Co., Ltd. Crude oil was provided by CQ Oilfield with a viscosity of 5 mPa s at 80 °C. The ionic composition of the simulated formation water from the CQ oilfield is shown in Table 2. Deionized water was produced by double distillation in the laboratory (resistivity = 18.4 M Ω cm).

2.2. Methods

2.2.1. Swelling rate

The swelling property of the microspheres is characterized by the swelling rate using the volume method (Tang et al., 2020). The 0.5 mL dry microsphere powder and 20 mL simulated formation water were added to a 25-mL test tube; the test tube was sealed and placed in an oven. The volume of the microspheres after swelling at different temperatures, salinities, pH values and hydration times was recorded. The swelling rate of the microspheres was calculated by Eq. (1).

$$R_{\rm S} = \frac{V_{\rm t}}{V_0} \tag{1}$$

where R_s is the swelling rate; V_t is the swelling volume of the microsphere, mL; V_0 is the initial volume of the microsphere, mL.

2.2.2. Rheological measurement

The apparent viscosity and shear viscosity of the microsphere dispersion were measured using an Anton Paar rheometer (Austria, MCR301) with the coaxial cylinder system (CC27). The rheometer was equipped with Peltier temperature control software, which could control the temperature error within $\pm 0.1~$ °C. Microsphere dispersions with mass concentrations of 0.1%, 0.3% and 0.5% were preheated at 80 °C for 10 min. The apparent viscosity of the microsphere dispersions was measured at a shear rate of 7.34 s⁻¹. The shear viscosity of the microsphere dispersions was measured at shear rates ranging from 0.1 to 4000 s⁻¹.

Due to the circular shape of the polymer microspheres, there is a slip phenomenon when using a rheometer flat plate system to test viscoelasticity. To avoid the problem of slip phenomenon, the plate visualization system of the rheometer (PP43) was used to test the viscoelasticity through the microsphere body gel (Yang et al., 2018). By using the dynamic oscillation method, the gap was set as half of

the body gel thickness, the frequency was fixed at 1.0 Hz and the strain was changed to test the linear platform of viscoelasticity. Particular strain was fixed in the linear platform and the viscoelasticity test was performed on the body gel in the frequency range of 0.1–10 Hz.

2.2.3. Stability

(1) Thermogravimetry (TGA)

Thermal stability of microspheres was tested using a thermogravimetric analyzer (China, HS-TGA-101). Among them, the nitrogen protective atmosphere was set, the test temperature range was set to $40-800~^{\circ}\text{C}$ and the heating gradient was set to $15~^{\circ}\text{C/min}$.

(2) Dispersibility

The microsphere dispersions with mass concentrations of 0.1%, 0.3%, and 0.5% were prepared by ultrasound to ensure thorough dispersion. Microscopic dispersions were tested using a Formulation Stability Analyzer (France, TURBISCAN Lab). Before testing, the dispersion was thoroughly shaken and placed in the instrument. The instrument temperature was set at 80 $^{\circ}$ C and the height of the sample was 50 mm. The sample was scanned every 2 min for 1 h. The Turbiscan stability index (TSI) value of the dispersion solution can determine the dispersion stability of microspheres. The TSI was calculated by Eq. (2).

$$I = \sqrt{\frac{\sum_{i=1}^{n} (x_i - x_{bs})^2}{n-1}}$$
 (2)

where I is the Turbiscan stability index, the higher the TSI value, the less stable the dispersed system; n is the scan times; x_i is the backscattered light intensity at the scan time of i; and x_{bs} is the average backscattered light intensity.

(3) Long term stability

Under high temperatures, high salinity and highly acidic environment (80 °C, 85,000 mg/L and pH = 3), DCNPM-A microsphere and SCNPM microsphere were placed in ampoule bottles and sealed in the oven for a long time. The microspheres were visually inspected periodically for fragmentation or deterioration to observe their long-term stability.

In order to quantitatively characterize the long-term stability strength of the microspheres, the viscoelasticity of the microspheres in the supercritical CO_2 state (80 °C, 8 MPa) was determined. Firstly, the viscoelasticity of the body gel was tested after water absorption. Secondly, the body gel was placed in a container resistant to high temperature, high pressure and CO_2 ; 1/2 volume of simulated formation water was added to the container and CO_2 was injected to 7 MPa. The container was placed in an oven at 80 °C, and under the effect of thermal expansion, the pressure exceeded 8 MPa, causing the CO_2 to be in a supercritical state. After 60 d, the viscoelasticity of the body gel was tested.

The body gel was prepared as follows (Yang et al., 2018). An initiator was added to the aqueous formulation of microspheres and poured into a homemade etching reaction container with

Table 2Composition of simulated formation water in CQ oilfield.

Ion	Ca ²⁺	Ba ²⁺	Na ⁺	HCO ₃	Cl-	Salinity
Concentration, mg/L	1506	5076.57	28745.17	129.48	49596.26	85053.48

dimensions of 150 mm \times 100 mm \times 3 mm (Fig. 1(a)). The container was sealed and allowed to react at 40 °C for 2 h to obtain the schistose body gel. The body gel was formed into a uniform cylindrical sheet with dimensions of 15 mm \times 3 mm (Fig. 1(b)) to obtain the sample for the viscoelasticity test.

2.2.4. Core flooding

(1) Injectability of microsphere dispersion

The experimental flowchart of the microsphere injection is shown in Fig. 2(a). An artificial core (Φ 2.5 cm \times 10 cm) containing unsaturated crude oil with different crack widths (0.03, 0.05, and 0.1 mm) was used for the experiment, as shown in Fig. 3. Microsphere dispersion with a concentration of 0.5% was continuously injected at a temperature of 80 °C and an injection rate of 0.5 mL/min. The differential pressure between the injection end and the production end was recorded in real time.

(2) Migration experiment

As shown in Fig. 2(b), a long fractured core model (Φ 2.5 cm \times 30 cm) with three pressure taps was used to investigate the migration of DCNPM-A microsphere dispersion. The pressure observation points were divided into injection point A, pressure points B and C on the core holder. The specific experimental procedures are as follows. A microsphere dispersion solution with a concentration of 0.5% was prepared for use. 2 PV formation water was injected and then the microsphere dispersion was transferred. The migration of microspheres was analyzed by the differential pressure change at three pressure measurement points.

(3) Relationship between plugging rate and enhanced oil recovery

The experimental process is shown in Fig. 2(a), where a fractured heterogeneous core model (Φ 2.5 cm \times 10 cm) was used to study CO₂ oil displacement and anti-gas channeling. The core was saturated with CQ oilfield crude oil at an experimental temperature of 80 °C. The confining pressure was set at 15 MPa and the backpressure at the end of the core holder was set at 8 MPa (to ensure supercritical CO₂ flooding). The CO₂ gas injection rate was fixed at 0.1 mL/min. The enhanced oil recovery effect was calculated at different plugging rates by varying the injection parameters (injection rate, injection quantity, etc.) of the DCNPM-A microsphere dispersion.





Fig. 1. Preparation molds and samples for body gel. (a) Reaction container; (b) Body gel.

3. Results and discussion

3.1. Swelling performance with different influence factors

The water swelling property of microspheres is a significant index to evaluate its plugging performance. This section investigated the swelling performances of DCNPM-A microspheres with various influencing factors compared with traditional microspheres. Based on previous studies and the exploration of current performance, the acid-resistance mechanism of the DCNPM-A microsphere was described. Fig. 4 shows the influence of temperature, hydration time, pH value and salinity on the swelling rate of the DCNPM-A microsphere.

3.1.1. Temperature

In Fig. 4(a), with the increase in temperature, the swelling rate of both microspheres was increased, and the DCNPM-A microsphere was always higher than that of the SCNPM-A microsphere. When the temperature was higher than 60 °C, the swelling change rate of the DCNPM-A microsphere was higher than that of the SCNPM-A microsphere, showing the characteristics of secondary swelling. Due to macromolecular crosslinking agent UCA, the DCNPM-A microsphere has strong crosslinking flexibility under the same crosslinking density. Therefore, the DCNPM-A microsphere has high water absorption below 60 °C. Above 60 °C, the ester bond in UCA is gradually broken, the crosslinking density of the DCNPM-A microsphere is decreased, and the internal network structure becomes loose, so its swelling rate will suddenly increase, resulting in secondary swelling.

3.1.2. Hydration time

In Fig. 4(b), the DCNPM-A microsphere showed delayed swelling in the water absorption time of 0.17–0.50 d. The previous research (Zhou et al., 2022a) thoroughly analyzed that the double-crosslinking structure made the microsphere possess the characteristics of delayed swelling, which was caused by the breakage of the unstable crosslinking agent inside the microsphere.

3.1.3. *pH* value

In Fig. 4(c), as the formation water acidity increased, the swelling rate of traditional DCNPM microspheres decreased, while DCNPM-A microspheres were less affected by pH value. It showed that DCNPM-A microspheres had excellent acid-resistance and were suitable for use in CO2 flooding reservoirs. For DCNPM microsphere, as the pH value decreased, i.e., the concentration of H⁺ increased, H⁺ was combined with the hydration groups -COO⁻ on the molecular chain, resulting in weakened hydration and molecular curling due to the decrease in repulsive force, which led to the weakening of the swelling performance and acid-resistance. However, the acid-resistant cationic monomer DMDAAC was introduced into the DCNPM-A microsphere. The cationic group existed on the molecular chain of the microsphere, and there was electrostatic repulsion between $-N^+$ and H^+ , making it is difficult for H⁺ to combine with the anionic group. To some extent, the acidresistance of the microsphere was achieved. On the other hand, the unstable crosslinking agent UCA could release -COO- after the ester bond was broken and decomposed, which could combine with H⁺ as a "sacrificial agent" to some extent to improve the acidresistance of the microsphere.

3.1.4. Salinity

In Fig. 4(d), with the increase in salinity, the swelling characteristics of the microspheres become worse, but the DCNPM-A microsphere still had a high swelling rate of 13.5 at the salinity of 85,000 mg/L. The electrical layer is compressed and thins as salinity

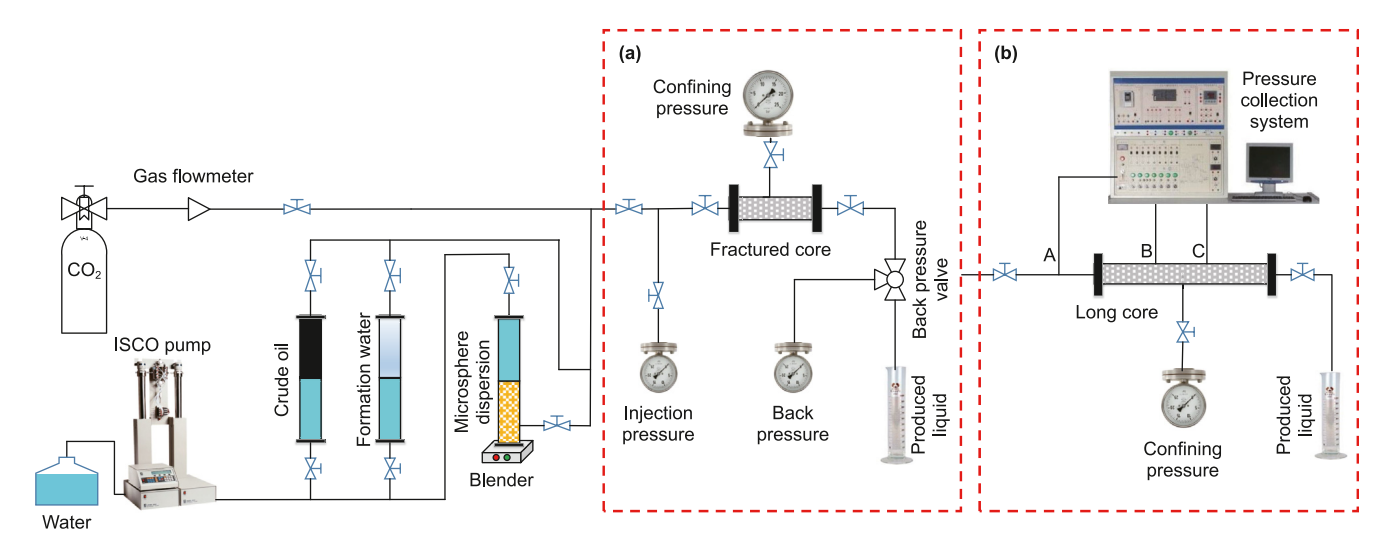


Fig. 2. Flow chart of the core displacement experiment.



Fig. 3. Artificial fractured core. (a) Top view; (b) Side view.

increases, causing the hydrodynamic radius of the microsphere to decrease and its swelling performance to worsen (< 25,000 mg/L) (Wang et al., 2022). With the further increase in salinity, the hydration layer and the double electric layer are further compressed. However, the more salt ions also penetrate the space structure of the microsphere, the higher the osmotic pressure inside and outside the structure, the more the free water enters the structure to increase the swelling. Under the influence of the compression of the hydration layer and the double electrical layer and the osmotic pressure, the overall swelling performance of the microsphere slows down compared to that at low salinity. However, the overall decrease still shows that the effect of osmotic pressure is less than that of the compressed double electric layer, so the swelling property of microspheres decreases slowly (25,000–80,000 mg/L).

In short, under the harsh conditions of 80 °C, 85,000 mg/L and pH = 3, the DCNPM-A microsphere has the characteristics of secondary expansion and delayed swelling. Under acidic conditions, DCNPM-A microsphere has better expansion performance than the traditional microsphere, which makes DCNPM-A microsphere has the characteristics of "low expansion factor migration near the well, high expansion factor plugging far well". It can penetrate the formation to achieve plugging under the control of temperature and time. It is beneficial to prevent CO_2 gas channeling in the far-well zone.

3.2. Acid-resistant mechanism

To establish the relationship between microstructure and performance, the micromorphology of the DCNPM-A microspheres at low and high temperatures was studied by atomic force microscopy (AFM). In the low temperature image (Fig. 5(a)), the highest peak

was 31.0 nm. The highest peak in the high temperature image (Fig. 5(b)) was 393.8 nm. The main reason for the above phenomenon was that in the AFM image, the deformation signal in the vertical direction reflected the change in sample shape. In the low temperature image, because the eater bond in the UCA was not broken, the crosslinking density of gel microspheres was dense, the three-dimensional network crosslinking structure was also dense and the peak height on the AFM image was low. In the high temperature image, the crosslinking structure of the three-dimensional network was weak due to the broken of the eater bond in UCA. Therefore, the AFM images at high temperatures showed higher peaks.

Based on the influencing factors of microsphere swelling property and its crosslinking images of AFM, the acid-resistant mechanism of DCNPM-A microsphere was proposed as follows.

On the one hand, the cationic charge causes the microsphere to absorb water and expand. Since there are carboxylate groups on the molecular chain of the traditional microsphere and the CO₂ flooding formation is acidic, the carboxylate radicals on the molecular chain combine with the free hydrogen ions in the formation water to form carboxylic acid, which causes the molecular chain of the microsphere to have no charge. The hydration ability and expansion performance become poor. DCNPM-A microspheres can achieve excellent expansion in acidic formation, and its acid-resistant mechanism is shown in Fig. 6. The cationic monomer DMDAAC is introduced into the DCNPM-A microsphere, and the molecular chain of the microsphere contains sulfonate and ammonium group, which can be formed into "internal salt bond". While the microsphere is in acidic formation, hydrogen ions are distributed in the outer layer of the sulfonate to form a double electrical layer to shield its anionic charge, and the "internal salt bond" is opened. The

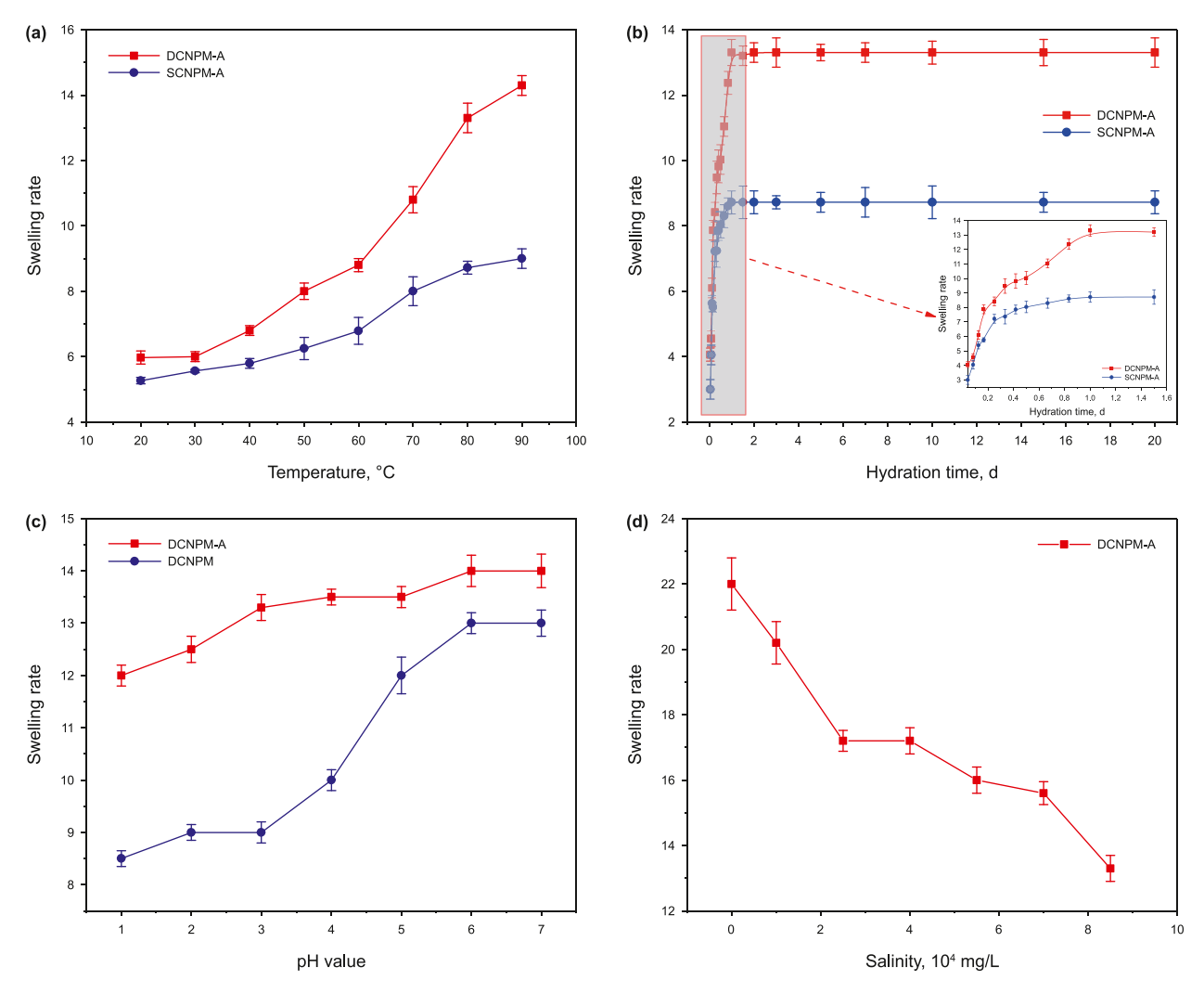


Fig. 4. Swelling performance of the DCNPM-A microsphere varies with different factors.

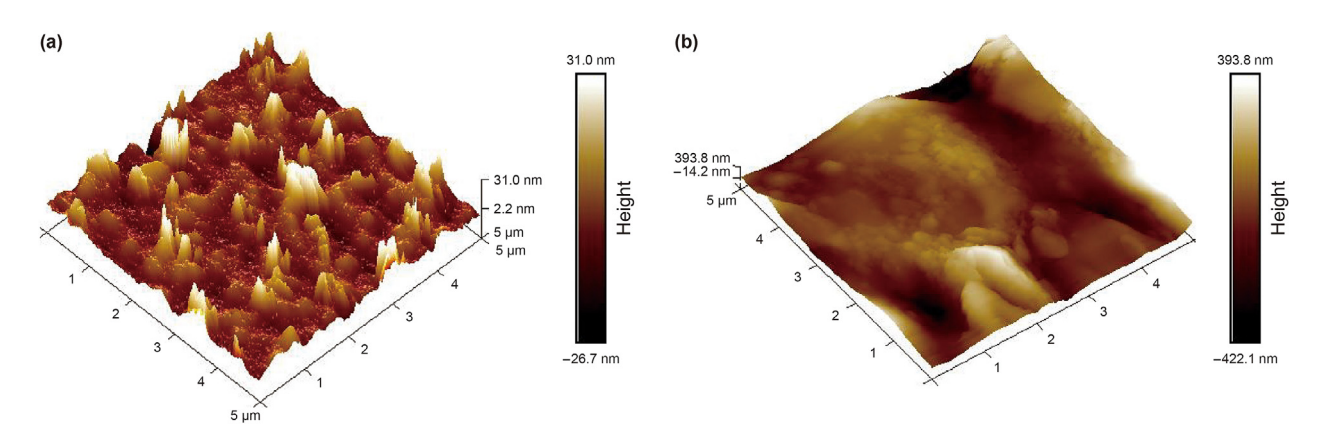


Fig. 5. AFM images of microsphere at low (a) and high (b) temperatures.

ammonium group is exposed on the molecular chain and osmotic pressure is created due to the charge imbalance inside and outside the microsphere, allowing the microsphere to absorb water and expand under acidic formation.

On the other hand, unstable crosslinking leads to secondary expansion of the microspheres. There are ester bonds in the

unstable crosslinking agent UCA. When the formation temperature reaches the ester bond breaking temperature, the internal crosslinking density of the microsphere decreases due to the breaking of ester bond. Therefore, the microsphere can absorb water and expand further in the acidic environment. The two aspects mentioned above improve the expandability of the microspheres

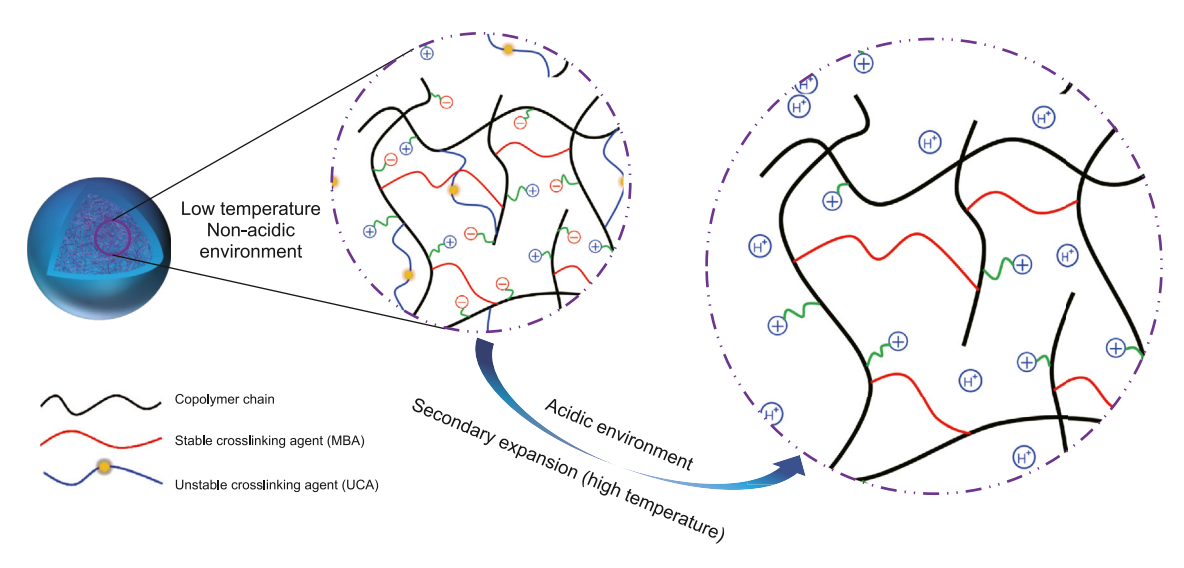


Fig. 6. Acid-resistant mechanism of the DCNPM-A microsphere.

during acidic formation and their acid-resistance.

3.3. Viscosity and injectability of microsphere dispersion

The low shear-viscosity and high injectivity are crucial for the field applications of microsphere dispersions during their pumping process. Thus, they need to be intrinsically investigated in the laboratory tests.

3.3.1. Dispersion viscosity

Viscosity affects the injectivity and migration of the profile control system. It is an essential index of microsphere dispersion. Moreover, the change in viscosity can reflect the microscopic force in the microsphere dispersion. Fig. 7 shows the viscosity—temperature curve of DCNPM-A microsphere dispersion at different concentrations. In the range of 25–90 °C, the dispersion viscosity is all lower than 1.4 mPa s. The dispersion viscosity shows a slow, rapid and stable trend with increasing temperature. Furthermore, the dispersion viscosity increases with the increase in concentration. At low temperatures, the microspheres have low expansion and high

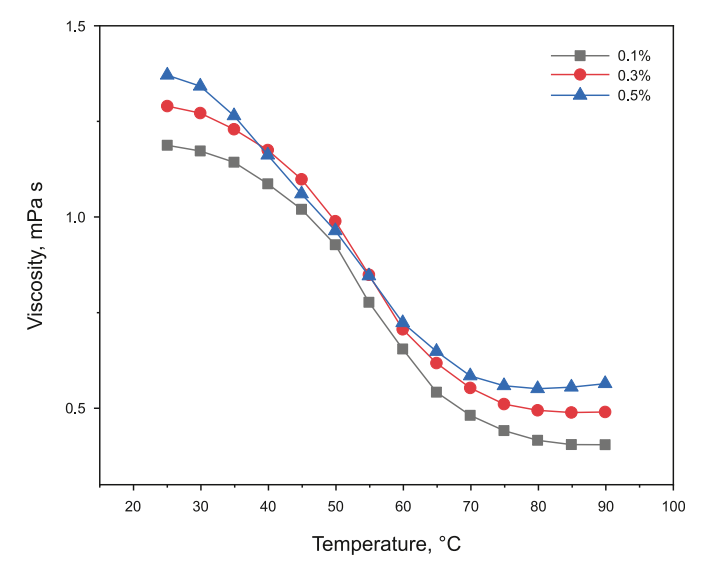


Fig. 7. Viscosity—temperature relationship of the DCNPM-A microsphere dispersion.

hardness, resulting in an enormous impact on the measuring rotor, and the molecular thermal movement is not violent. Hence, the microspheres are mostly aggregated and the dispersion viscosity is high. In the range of 25–40 °C, as the temperature increases, the hardness of the microspheres becomes lower due to the increased hydration ability, and the dispersion viscosity shows a slight decreasing trend. In the range of 40–70 °C, the temperature is higher, the molecular thermal movement is intensified and the dispersion of microspheres is better, so the viscosity change rate is fast. In the range of 70–90 °C, the microsphere exhibits secondary and complete expansion. The temperature has little effect on the dispersion viscosity, so the viscosity tends to be stable. Li et al. (2015) proposed a mechanism of "entanglement thickening" for the outer layer of microspheres. The polymer chain layer outside the microsphere is relatively loose, and weak mutual penetration can occur between two microspheres, resulting in entanglement. Therefore, the dispersion viscosity will increase with the "entanglement thickening". There is a critical concentration of "entanglement thickening". Above this concentration, the entanglement of the microspheres and the osmotic compression of the anti-ions will reduce the specific volume and viscosity of the microspheres. It can be seen from Fig. 4 that this phenomenon is more evident at 40-60 °C. At this point, the entanglement mechanism plays a leading role. As the concentration of microsphere dispersion increases from 0.1% to 0.3%, the entanglement mechanism is conducive to the increase in viscosity. When the concentration increased from 0.3% to 0.5%, the critical concentration was exceeded, resulting in a decrease in the specific volume and viscosity of the microspheres due to the entanglement mechanism. When the temperature is higher than 60 °C, the molecular thermal motion dominates and the microspheres are not easily entangled, so the viscosity increases with the increase in concentration.

3.3.2. Shear thickening

During injection and migration, microspheres are subjected to the shear action of the wellbore and formation. The viscosity of the microsphere dispersion is influenced by the shear rate magnitude, which subsequently affects injection and migration. The effect of the shear rate on the viscosity of the microsphere dispersion is mainly investigated in this section. Fig. 8 shows the viscosity of DCNPM-A microsphere dispersion at various temperatures and concentrations as a function of shear rate. The viscosity of the microsphere dispersion decreased initially and then increased as

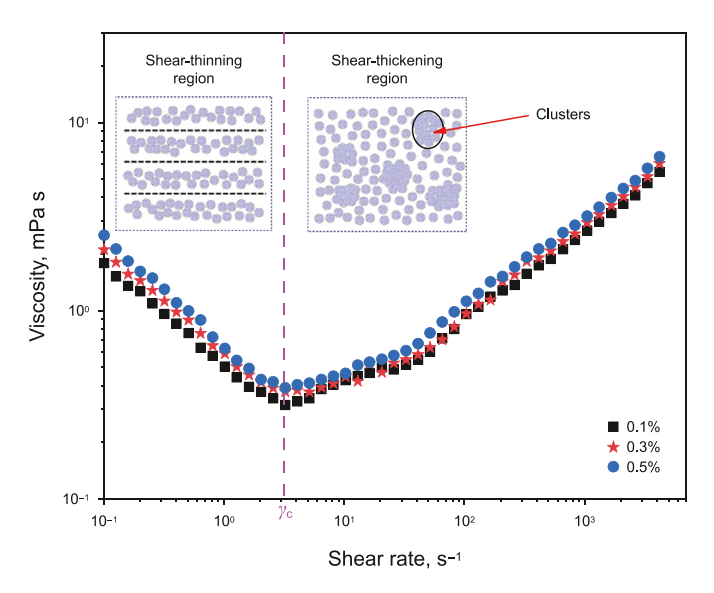


Fig. 8. Shear viscosity of the DCNPM-A microsphere dispersion.

the shear rate increased. The shear viscosity of the microsphere dispersion exhibits shear thinning followed by shear thickening, with a critical shear rate (γ_c) (Yang H. et al., 2015, 2019). The viscosity increases with concentration and decreases with temperature.

The microsphere dispersion exhibits thinning and shear thickening, which can be attributed to the internal interaction force under steady shear. Fig. 8 shows that the microsphere dispersion exhibits a layered ordered body when the shear rate is lower than γ_c , in accordance with the theory of Hoffman dispersion system layered structure. There is no interaction between the layers at low shear rates. When the shear rate is increased further, the microsphere particles move irregularly and finitely in the layer, indicating a shear-thinning pseudoplastic fluid. While the shear rate surpasses γ_c , the microsphere particles make contact, leading to the formation of a concentrated "particle cluster" as they overcome the interaction force. The "particle cluster" increases in size as the shear increase, causing disruption in the interlayer flow and resulting in shear thickening. As the concentration of microspheres increases, the internal friction between them also increases, resulting in higher flow resistance and increased viscosity of the fluid.

Generally, in the concentration range of 0.1%-0.5%, the dispersion viscosity is lower at the shear rate below $100~\text{s}^{-1}$. To ensure the low viscosity of the dispersion used in the oilfield, the concentration of the dispersion can be increased to 0.5% at a shear rate below $100~\text{s}^{-1}$.

3.3.3. Fractured core injectability

The core parameters used to investigate the injectability of DCNPM-A microspheres in fractured cores with varying crack widths are listed in Table 3. The permeability of the matrix core is all $10\times10^{-3}~\mu\text{m}^2.$ When the crack width is 0.10, 0.05 and 0.03 mm, the permeability of the fractured core is 849.26 \times 10 $^{-3}$, 70.77 \times 10 $^{-3}$, 28.31 \times 10 $^{-3}$ μm^2 , respectively. Fig. 9 shows the

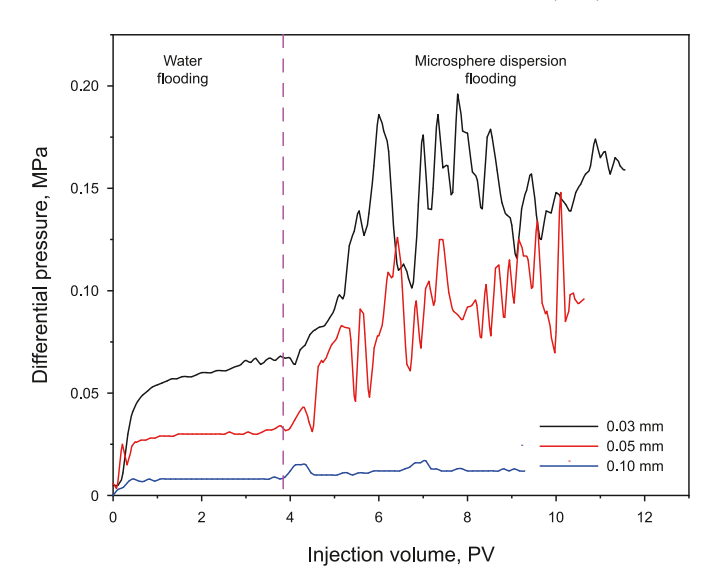


Fig. 9. Differential pressure of DCNPM-A microsphere in fractured cores with different slit widths.

injection pressure of DCNPM-A microsphere dispersion in fractured cores. The injection pressure increased during both water flooding and microsphere flooding as the crack width decreased. The pressure change observed during microsphere flooding with a crack width of 0.1 mm is comparable to that of water flooding. This suggests that the DCNPM-A microspheres were not effective in retaining and blocking the crack, resulting in an extremely poor core plugging effect. While the crack widths were 0.05 and 0.03 mm, the temporary plugging rates of DCNPM-A microspheres were 68.57% and 78.45%, respectively, indicating that the microspheres had better temporary plugging ability for fractured cores with a crack width of 0.03 mm. Although microspheres become less injectable as the crack width decreases, they can still be transported through adsorption, retention, aggregation and bridging in the 0.03 mm fractured core for plugging purposes. In summary, the DCNPM-A microspheres exhibit positive injectability in the fractured core, even with a crack width as small as 0.03 mm.

3.4. Stability performance of the microsphere dispersion

Profile control is a long-term engineering challenge. Plugging agents can only ensure their long-term effectiveness underground if there is extremely high stability. This section focuses on the stability performance of microspheres under different conditions.

3.4.1. Thermal stability

Fig. 10 shows the thermogravimetric (TGA) curves of DCNPM-A and SCNPM microspheres. According to Table 4, the thermal stability of the DCNPM-A microsphere was higher than that of the SCNPM microsphere. The thermal degradation of the DCNPM-A microsphere occurs in three stages. During the first stage, which ranged from 40 to 250 °C, the mass loss was primarily due to the evaporation of bound water inside the microsphere, ester bond

Table 3Fractured core parameters of injectivity experiments.

Core No.	Crack width, mm	Porosity, %	Permeability, 10 ⁻³ μm ²	Plugging rate, %
10-001	0.10	20.38	849.26	–
10-002	0.05	19.36	70.77	68.57
10-003	0.03	18.24	28.31	78.45

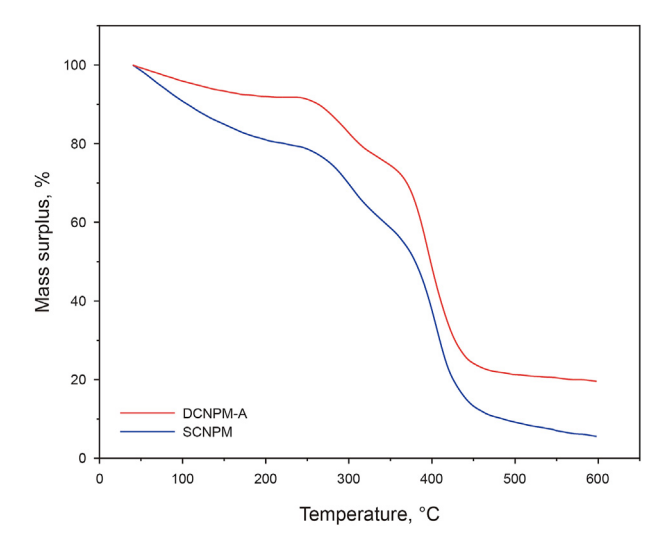


Fig. 10. TGA curves of two types of microspheres.

Table 4Thermal performance data of two types of microspheres.

Type of microsphere	Remaining mass at different temperatures, %			
	250 °C	450 °C	600 °C	
DCNPM-A SCNPM	91.37 78.73	24.04 13.06	18.53 5.6	

breakage of the UCA crosslinking agent, and thermal degradation of oligomers. The second stage occurred between 250 and 450 °C, during which the mass loss was primarily due to the decomposition of the side groups (-NH₂, -COO⁻, -SO₃ and benzene ring) on the backbone of the microsphere molecule. The third stage was between 450 and 600 °C, the backbone of the microsphere molecule broke down, the MBA crosslinking bonds broke, and the threedimensional network skeleton structure collapsed, resulting in significant mass loss. The mass of remaining DCNPM-A microspheres was ultimately 18.53%, significantly higher than the 5.6% of SCNPM microspheres. The functional groups in the microsphere molecular structure contribute to the higher thermal stability of DCNPM-A microspheres compared to traditional microsphere. The DCNPM-A microsphere contains two temperature-resistant functional groups: the sulfonic acid group and the rigid benzene ring. These groups have lower temperature sensitivity, which increases the temperature resistance of the DCNPM-A microsphere to some extent.

3.4.2. Dispersion stability

Yang et al. (2017) proposed using a stability analyzer to test the TSI value of microsphere dispersion to evaluate its particle stability. It is pointed out that as the temperature increases, the viscosity of the microsphere dispersion system decreases and the microsphere particles tend to sink, resulting in instability of the whole system and an increase in the TSI value. This study uses the TSI value as an evaluation indicator and a stability analyzer to test the dispersion stability of DCNPM-A microsphere with different concentrations at various temperatures. As shown in Fig. 11, the TSI value of the microsphere dispersion increased with time, concentration and temperature. This indicated that the microsphere dispersion underwent partial sedimentation and aggregation with the increases in time and concentration, resulting in poor stability. As the temperature increased, the thermal motion of the nanoparticles

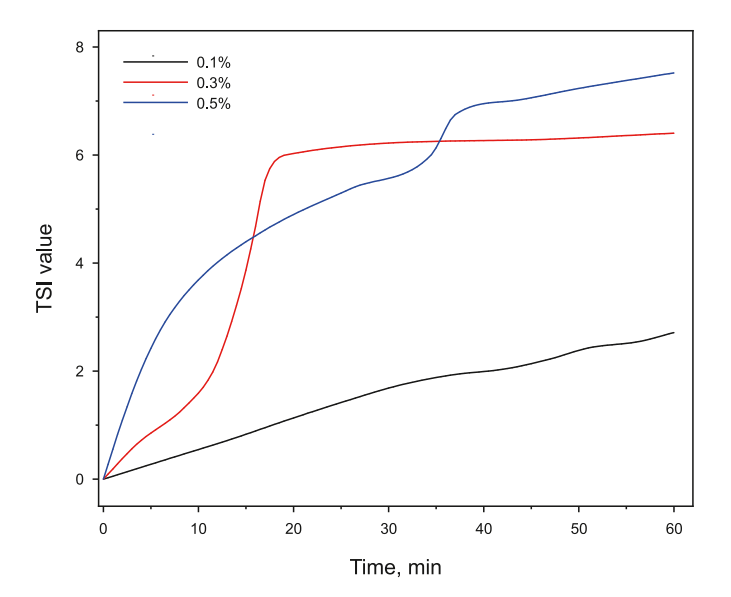
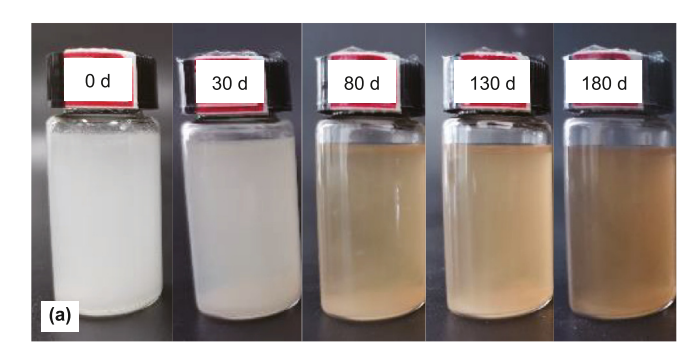


Fig. 11. Dispersion stability of DCNPM-A microsphere dispersion.

intensified, leading to an increase in collision and aggregation opportunities, and a subsequent deterioration in stability. However, the TSI values of the dispersions at all three concentrations were below 8, indicating that DCNPM-A microspheres exhibited good dispersion stability at concentrations below 0.5%. The microsphere dispersion has good dispersibility within a short period at a concentration of 0.5% or less. This characteristic enables the microsphere to maintain a good suspension dispersion near the wellbore and to penetrate deep into the formation for plugging under seepage action, facilitating its deep migration.

3.4.3. Long-term stability

A long-term static stability evaluation of DCNPM-A and SCNPM microspheres was conducted under high temperature, high salinity, and highly acidic environments. A 1% microsphere dispersion was prepared using CQ oilfield simulated formation water (pH = 3) and placed in an 80 °C oven. The experimental results are shown in Fig. 12. At 0 d, both microspheres were well dispersed in the formation water, resulting in an overall opaque white dispersion. After 30 d, the SCNPM microsphere showed a semi-suspended state, with some solid particles settling and the solution appearing opaque. The DCNPM-A microspheres settled to the bottom, and the solution appeared transparent. From the 80th to the 180th day, the SCNPM microsphere dispersion tended to be uniform, suggesting that they gradually degraded and became more unstable in high temperature, high salinity, and highly acidic environments. The stability of DCNPM-A microspheres is consistently good due to the addition of acid-resistant monomer DMDAAC, the presence of temperature- and salt-resistant sulfonic acid functional group, and the rigid benzene ring. Additionally, the microspheres settled well on the bottom without degradation. After shaking the ampoule, the microsphere particles were in a uniform suspension state and remained suspended for a certain period without sinking. This indicates that the sedimentation of microsphere particles under longterm static conditions is a dynamic instability and represents an aggregated state. Under actual geological flow conditions, the microspheres are dispersed and relatively dynamically stable. Therefore, in practical geological applications, the microspheres do not excessively deposit during the seepage process, causing only minor blockage damage to the matrix formation of low-permeability reservoirs. In summary, DCNPM-A microspheres exhibit excellent



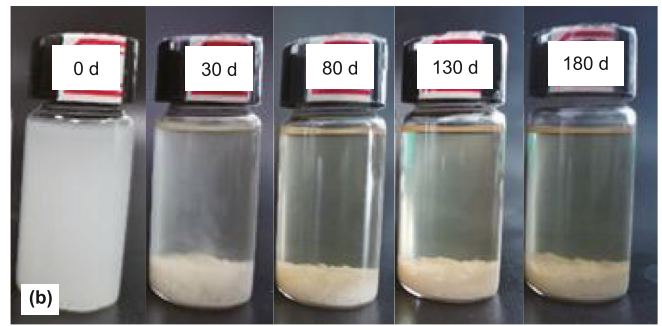


Fig. 12. Long-term stability in high temperature, high salinity and acidic environment. (a) SCNPM microsphere; (b) DCNPM-A microsphere.

stability in high temperature, high salinity, and highly acidic environments, without any degradation. They also demonstrate good long-term stability.

As shown in Fig. 13, the viscoelasticity of DCNPM-A microsphere bulk gel was tested after water absorption and after being placed in a supercritical CO_2 state for 60 d. The viscoelasticity of bulk gel reflects its ability to deform after strain. The storage modulus (G') represents elasticity and reflects the difficulty of elastic deformation of the microspheres. In contrast, the loss modulus (G') represents viscosity and reflects the ability to dissipate during deformation.

It can be seen that when the bulk gel absorbed water and expanded, it had a greater viscoelasticity and G' > G'', indicating that the microsphere was an elastic particle. When the bulk gel was placed in a supercritical CO₂ state for 60 d, its G' decreased compared to before, while G' increased. This situation arises because, in the supercritical CO₂ state, the pressure and temperature reach 8 MPa and 80 °C, respectively. The high pressure causes the supercritical CO₂ to dissolve in water and reach a dissolution equilibrium within 60 d. The effect of acid corrosion causes damage and degradation to the microsphere structure, resulting in a decrease in G' and a slight increase in G''. However, the decrease in the amplitude of G' and the increase in the amplitude of G'' are small. This is mainly due to the fact that under high pressure, the probability of mutual coverage and overlap between polymer molecules increases, resulting in a denser network structure. This, to some extent, weakens the damage caused by acid corrosion to

Table 5Fractured core parameters for exploring the deep migration.

Core No.	Porosity, %	Crack width, mm	Permeability, $10^{-3} \mu m^2$	
30-003	16.98	0.03	67.05	

the network structure, resulting in a small decrease in amplitude. Overall, the DCNPM-A microspheres have excellent resistance to the supercritical CO_2 state and can maintain stability in this state for at least 60 d.

3.5. Deep migration in core

DCNPM-A microspheres are acid-resistant microspheres with delayed swelling behavior. The delayed swelling characteristics of DCNPM-A microspheres under static conditions have been discussed in previous works. In this section, the delayed swelling of the microsphere during its deep migration is mainly investigated.

Table 5 shows the long core parameters used to investigate the migration, and Fig. 14 shows the pressure changes at three pressure taps (A, B and C) during the migration process of DCNPM-A microspheres. DCNPM-A microsphere dispersion was injected after water flooding of 2 PV. Due to the presence of a migration front after microsphere injection, the corresponding pressure gradually increased as the migration front moved toward the pressure measurement point. Therefore, there was a relaxation in the pressure

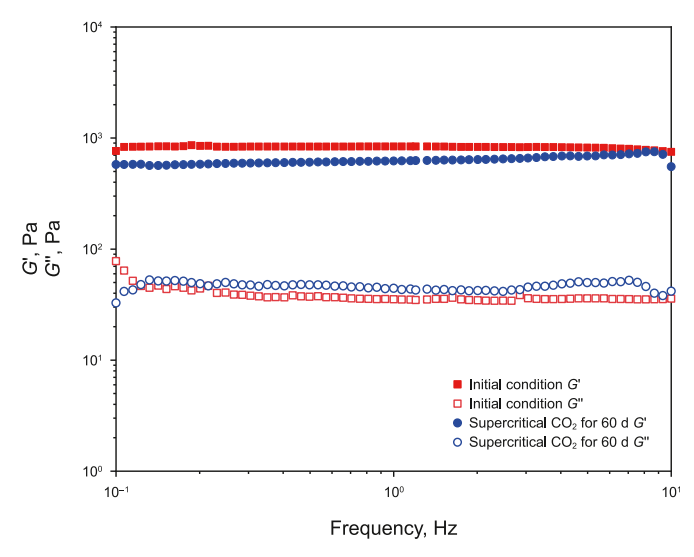


Fig. 13. Effect of supercritical CO₂ on the dynamic modulus of DCNPM-A.

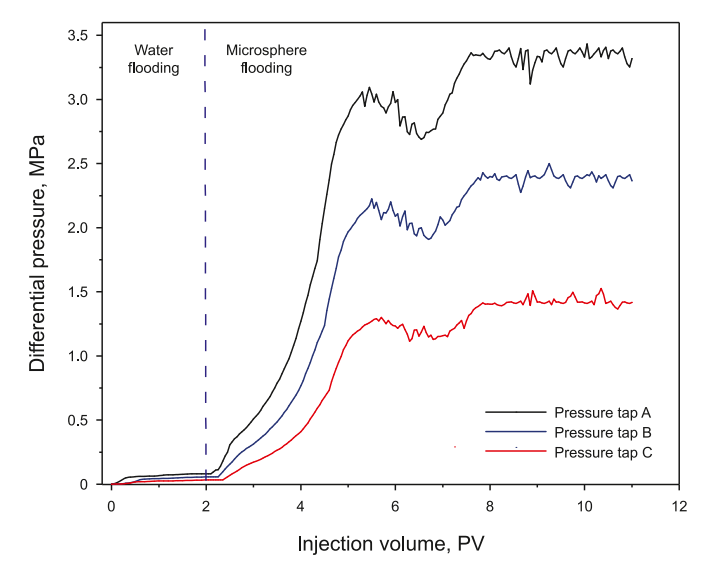


Fig. 14. Pressure change curves of DCNPM-A microsphere in deep migration.

rise of the two pressure taps B and C. During the injection process of microsphere dispersion, the pressure tended to increase and stabilize, but there was a period of a sudden pressure drop and then the increase in the 5.5 to 7.8 PV. Based on the trend observed at all three pressure measurement points, there was a blockage of microsphere aggregation after the pressure measurement point C. However, as the injection progressed, the aggregation block gradually receded until the pressure suddenly dropped after removal from the production end. After 8 PV, the pressure gradually stabilized, indicating that the delayed swelling characteristic of the microspheres was reflected. At this point, the temperature and hydration time had reached the conditions for secondary swelling, improving the ability of microsphere to plug the cracks. As a result, the subsequent injection pressure increased and stabilized. The pressure fluctuated continuously throughout the injection process of DCNPM-A microsphere dispersion, indicating that the microspheres exhibited a dynamic plugging process of "migration, plugging, remigration, secondary expansion and replugging". This migration facilitated the penetration of the microsphere deep into the formation for plugging.

3.6. Plugging performance and enhanced oil recovery

Previous research indicates that microsphere dispersions with a concentration ranging from 0.1% to 0.5% exhibit good injectability. In this study, a concentration of 0.5% was used to investigate the plugging performance to reduce the volume of the injected dispersion. The relationship between microsphere plugging rate and enhanced oil recovery by CO₂ flooding was obtained by altering the injection parameters of DCNPM-A microsphere dispersion, as shown in Fig. 15.

As the plugging rate of the microspheres increased, the effect of enhanced oil recovery also increased. However, in cases of excessive plugging, the extent of enhanced oil recovery decreased. This is because the increased plugging strength of the microspheres leads to an increase in the contact area between the microspheres and the crack after aggregation, which in turn decreases the opportunity for subsequent displacement fluid to pass through the microspheres and the crack wall. Therefore, improving crack heterogeneity is ideal for enhanced oil recovery. If the plugging rate is too high, some microsphere particles may enter the matrix core, reducing the contact between the subsequent displacement fluid

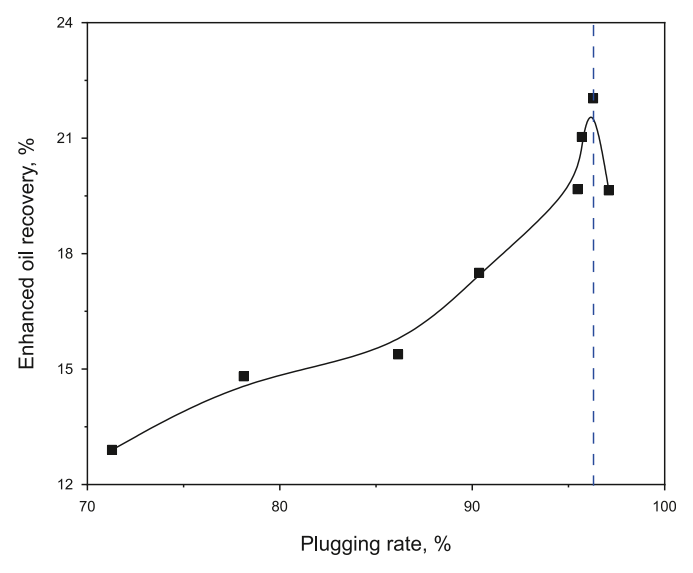


Fig. 15. Relationship between plugging rate and enhanced oil recovery.

and the crude oil in the matrix, thus reducing the effectiveness of enhanced oil recovery. Based on the long-term stability of microspheres in the supercritical CO₂ state, it was found that although the volume of microspheres increased after water absorption, the decrease in their elastic modulus was relatively small. This indicates that they still maintain high strength in the supercritical CO₂ state. The impact of strength reduction on plugging ability was minimal. As a result, the microspheres demonstrated exceptional capacity in regulating crack heterogeneity. To achieve optimal plugging and anti-gas channeling effects at the oilfield site and to enhance oil recovery more effectively, it is recommended to maintain a plugging rate of approximately 95%.

4. Conclusions

- (1) DCNPM-A microspheres exhibit secondary swelling at 70 °C. The swelling rate is 13.5 (in 85,000 mg/L formation water (pH = 3) and 80 °C), which is higher than that of traditional microsphere.
- (2) The mechanism of acid-resistance in DCNPM-A microspheres has been elucidated. In acidic conditions, the internal salt bond of the microspheres is destroyed, and secondary expansion contributes to the improved acidresistance.
- (3) The TSI values of the DCNPM-A microsphere dispersion are all below 8, indicating good dispersion stability. When the viscosity is below 1.5 mPa s, the dispersion has good injectability. The final optimized concentration of the DCNPM-A microsphere dispersion is 0.5%.
- (4) The long-term stability of DCNPM-A microspheres exceeds 180 d in high temperature, high salinity, and highly acidic environments. In supercritical ${\rm CO_2}$ state, the stability can reach up to 60 d.
- (5) DCNPM-A microspheres exhibit secondary expansion characteristics during dynamic deep migration, which can effectively plug the formation and enhance oil recovery in CO₂ flooding under acidic reservoir conditions. To achieve high recovery efficiency in CO₂ flooding, it is important to control the microsphere plugging rate at 95%.

CRediT authorship contribution statement

Hai-Zhuang Jiang: Writing — review & editing, Writing — original draft, Investigation, Data curation. Hong-Bin Yang: Writing — review & editing, Writing — original draft, Funding acquisition, Conceptualization. Ruo-Sheng Pan: Validation. Zhen-Yu Ren: Visualization. Wan-Li Kang: Writing — review & editing, Writing — original draft, Funding acquisition, Conceptualization. Jun-Yi Zhang: Methodology, Investigation. Shi-Long Pan: Methodology, Investigation. Bauyrzhan Sarsenbekuly: Writing — review & editing, Writing — original draft.

Declaration of competing interest

No conflict of interest exits in the submission of this manuscript, and manuscript is approved by all authors for publication. I would like to declare on behalf of my co-authors that the work described was original research that has not been published previously, and not under consideration for publication elsewhere, in whole or in part. All the authors listed have approved the manuscript that is enclosed.

Acknowledgements

The project was supported by the Fund of State Key Laboratory of Deep Oil and Gas, China University of Petroleum (East China) (SKLDOG2024-ZYRC-06), Key Program of National Natural Science Foundation of China (52130401), National Natural Science Foundation of China (52104055, 52250410349), Major Science and Technology Project of China National Petroleum Corporation Limited (2021ZZ01-08) and Shandong Provincial Natural Science Foundation, China (ZR2021ME171).

Appendix A. Supplementary data

Supplementary data to this article can be found online at https://doi.org/10.1016/j.petsci.2024.02.002.

References

- Amir, Z., Saaid, I.M., Jan, B.M., et al., 2022. PAM/PEI polymer gel for water control in high-temperature and high-pressure conditions: core flooding with crossflow effect. Kor. J. Chem. Eng. 39 (3), 605–615. https://doi.org/10.1007/s11814-021-1006-y.
- Canbolat, S., Parlaktuna, M., 2019. Polymer gel conformance on oil recovery in fractured medium: visualization and verification. J. Petrol. Sci. Eng. 182, 106289. https://doi.org/10.1016/j.petrol.2019.106289.
- Dai, C., Liu, P., Gao, M., et al., 2022. Preparation and thickening mechanism of copolymer fluorinated thickeners in supercritical CO₂. J. Mol. Liq. 360, 119563. https://doi.org/10.1016/j.molliq.2022.119563.
- Ding, M., Li, Q., Yuan, Y., et al., 2022. Permeability and heterogeneity adaptability of surfactant-alternating-gas foam for recovering oil from low-permeability reservoirs. Petrol. Sci. 19 (3), 1185–1197. https://doi.org/10.1016/ i.petsci.2021.12.018.
- Du, D., Zou, B., Pu, W., et al., 2022. Injectivity and plugging characteristics of CO₂-responsive gel particles for enhanced oil recovery in fractured ultra-low permeability reservoirs. J. Petrol. Sci. Eng. 214, 110591. https://doi.org/10.1016/i.petrol.2022.110591.
- Elsharafi, M.O., Bai, B., 2016. Influence of strong preformed particle gels on low permeable formations in mature reservoirs. Petrol. Sci. 13 (1), 77–90. https://doi.org/10.1007/s12182-015-0072-3.
- Elsharafi, M.O., Bai, B., 2017. Experimental work to determine the effect of load pressure on the gel pack permeability of strong and weak preformed particle gels. Fuel 188, 332–342. https://doi.org/10.1016/j.fuel.2016.10.001.
- Gandomkar, A., Torabi, F., Riazi, M., 2021. CO₂ mobility control by small molecule thickeners during secondary and tertiary enhanced oil recovery. Can. J. Chem. Eng. 99 (6), 1352–1362. https://doi.org/10.1002/cjce.23936.
- Guzmán-Lucero, D., Martinez-Palou, R., Palomeque-Santiago, J., et al., 2022. Water control with gels based on synthetic polymers under extreme conditions in oil wells. Chem. Eng. Technol. 45 (6), 998–1016. https://doi.org/10.1002/ ceat.202100648.
- He, L., Shen, P., Liao, X., et al., 2015. Potential evaluation of CO₂ flooding for EOR and sequestration in YL oilfield of China. Int. J. Glob. Warming 8 (3), 436–451. https://doi.org/10.1504/I/GW.2015.072663.
- Ji, W., Dai, C., Cao, Y., et al., 2023. A novel CO₂-resistant dispersed particle gel for gas channeling control in low-permeability reservoirs. J. Mol. Liq. 374, 121251. https://doi.org/10.1016/j.molliq.2023.121251.
- Kang, W., Jiang, H., Yang, H., et al., 2021. Study of nano-SiO₂ reinforced CO₂ foam for anti-gas channeling with a high temperature and high salinity reservoir. J. Ind. Eng. Chem. 97, 506-514. https://doi.org/10.1016/j.jiec.2021.03.007.
- Li, Q., Liu, X., Zhang, J., et al., 2014. A novel shallow well monitoring system for CCUS: with application to Shengli Oilfield CO₂-EOR project. Energy Proc. 63, 2056, 2062, https://doi.org/10.1016/j.org/pro.2014.11.425
- 3956–3962. https://doi.org/10.1016/j.egypro.2014.11.425. Li, G., Ge, J., Zhang, G., et al., 2015. Viscosity characteristics of cationic polyacrylamide microsphere. J. China Uni. Petro. 39 (1), 176–181. https://doi.org/10.3969/j.issn.1673-5005.2015.01.026 (in Chinese).
- Li, Q., Ma, J., Li, X., et al., 2018. Integrated monitoring of China's Yanchang CO₂-EOR demonstration project in Ordos Basin. Energy Proc. 154, 112–117. https://doi.org/10.1016/j.egypro.2018.11.019.
- Liu, Y., Yang, J., Wu, T., et al., 2020. Pore-scale investigation on the plugging behavior of submicron-sized microspheres for heterogeneous porous media with higher permeability. Geofluids, 8869760. https://doi.org/10.1155/2020/8869760.
- Liu, S., Ren, B., Li, H., et al., 2022. CO₂ storage with enhanced gas recovery (CSEGR): a review of experimental and numerical studies. Petrol. Sci. 19 (2), 594–607. https://doi.org/10.1016/j.petsci.2021.12.009.
- Luo, X., Zheng, P., Gao, K., et al., 2021. Thermo- and CO₂-triggered viscosifying of aqueous copolymer solutions for gas channeling control during water-alternating-CO₂ flooding. Fuel 291, 120171. https://doi.org/10.1016/ j.fuel.2021.120171.
- Lv, \dot{H} ., Wang, L., Liu, G., et al., 2021a. Risk assessment on the CCUS project using risk breakdown structure methodology: a case study on Jilin oilfield CO_2 -EOR Hei-

- 79 block. Greenhouse Gas: Sci. Technol. 11 (4), 750–763. https://doi.org/10.1002/ghg.2077.
- Lv, Q., Zhou, T., Zheng, R., et al., 2021b. CO₂ mobility control in porous media by using armored bubbles with silica nanoparticles. Ind. Eng. Chem. Res. 60 (1), 128–139. https://doi.org/10.1021/acs.ject.0c05648.
- Nguele, R., Omondi, B.A., Yamasaki, S., et al., 2021. Evaluation of CO₂-triggered and thermo-responsive gels for heterogeneous oil formations. Colloids Surf. A Physicochem. Eng. Asp. 622, 126688. https://doi.org/10.1016/j.colsurfa.2021.126688.
- Pal, N., Zhang, X., Ali, M., et al., 2022. Carbon dioxide thickening: a review of technological aspects, advances and challenges for oilfield application. Fuel 315, 122947. https://doi.org/10.1016/ji.fuel.2021.122947.
- Paul, T., Bai, B., 2015. A more superior preformed particle gel with potential application for conformance control in mature oilfields. J. Pet. Explor. Prod. Technol. 5 (2), 201–210. https://doi.org/10.1007/s13202-014-0136-8.
- Pu, W., Du, D., Fan, H., et al., 2021. CO₂-responsive preformed gel particles with interpenetrating networks for controlling CO₂ breakthrough in tight reservoirs. Colloids Surf. A Physicochem. Eng. Asp. 613, 126065. https://doi.org/10.1016/ i.colsurfa.2020.126065.
- Rahmani, O., 2018. Mobility control in carbon dioxide-enhanced oil recovery process using nanoparticle-stabilized foam for carbonate reservoirs. Colloids Surf. A Physicochem. Eng. Asp. 550, 245–255. https://doi.org/10.1016/j.colsurfa.2018.04.050.
- Ren, B., Duncan, I.J., 2021. Maximizing oil production from water alternating gas (CO₂) injection into residual oil zones: the impact of oil saturation and heterogeneity. Energy 222, 119915. https://doi.org/10.1016/j.energy.2021.119915.
- Ren, B., Ren, S., Zhang, L., et al., 2016. Monitoring on CO₂ migration in a tight oil reservoir during CCS-EOR in Jilin Oilfield China. Energy 98, 108–121. https:// doi.org/10.1016/j.energy.2016.01.028.
- Ren, B., Male, F., Duncan, I.J., 2022. Economic analysis of CCUS: accelerated development for CO₂ EOR and storage in residual oil zones under the context of 45Q tax credit. Appl. Energy 321, 119393. https://doi.org/10.1016/j.apenergy.2022.119393.
- Risal, A.R., Manan, M.A., Yekeen, N., et al., 2019. Experimental investigation of enhancement of carbon dioxide foam stability, pore plugging, and oil recovery in the presence of silica nanoparticles. Petrol. Sci. 16 (2), 344–356. https:// doi.org/10.1007/s12182-018-0280-8.
- Shen, H., Yang, Z., Li, X., et al., 2021. CO₂-responsive agent for restraining gas channeling during CO₂ flooding in low permeability reservoirs. Fuel 292, 120306. https://doi.org/10.1016/j.fuel.2021.120306.
- Song, T., Zhai, Z., Liu, J., et al., 2022. Laboratory evaluation of a novel self-healable polymer gel for CO₂ leakage remediation during CO₂ storage and CO₂ flooding. Chem. Eng. J. 444, 136635. https://doi.org/10.1016/j.cej.2022.136635.
- Suicmez, V.S., 2019. Feasibility study for carbon capture utilization and storage (CCUS) in the Danish North Sea. J. Nat. Gas Sci. Eng. 68, 102924. https://doi.org/ 10.1016/j.jngse.2019.102924.
- Tang, X., Zhou, B., Chen, C., et al., 2020. Regulation of polymerizable modification degree of nano-SiO₂ and the effects on performance of composite microsphere for conformance control. Colloids Surf. A Physicochem. Eng. Asp. 585, 124100. https://doi.org/10.1016/j.colsurfa.2019.124100.
- Wang, Q., Yang, S., Lorinczi, P., et al., 2020. Experimental investigation of oil recovery performance and permeability damage in multilayer reservoirs after CO₂ and water—alternating-CO₂ (CO₂-WAG) flooding at miscible pressures. Energy Fuels 34 (1), 624–636. https://doi.org/10.1021/acs.energyfuels.9b02786.
- Wang, J., Kang, W., Yang, H., et al., 2022. Study on salt tolerance mechanism of hydrophobic polymer microspheres for high salinity reservoir. J. Mol. Liq. 368, 120639. https://doi.org/10.1016/j.molliq.2022.120639.
- Yang, H., Kang, W., Zhao, J., et al., 2015. Energy dissipation behaviors of a dispersed viscoelastic microsphere system. Colloids Surf. A Physicochem. Eng. Asp. 487, 240–245. https://doi.org/10.1016/j.colsurfa.2015.09.049.
- Yang, H., Kang, W., Yu, Y., et al., 2017. A new approach to evaluate the particle growth and sedimentation of dispersed polymer microsphere profile control system based on multiple light scattering. Powder Technol. 315, 477–485. https://doi.org/10.1016/j.powtec.2017.04.001.
- Yang, H., Kang, W., Tang, X., et al., 2018. Gel kinetic characteristics and creep behavior of polymer microspheres based on bulk gel. J. Dispersion Sci. Technol. 39 (12), 1808–1819. https://doi.org/10.1080/01932691.2018.1462192.
- Yang, H., Shao, S., Zhu, T., et al., 2019. Shear resistance performance of low elastic polymer microspheres used for conformance control treatment. J. Ind. Eng. Chem. 79, 295—306. https://doi.org/10.1016/j.jiec.2019.07.005.
- Yang, H., Lv, Z., Li, Z., et al., 2023a. Laboratory evaluation of a controllable self-degradable temporary plugging agent in fractured reservoir. Phys. Fluids 35 (8), 083314. https://doi.org/10.1063/5.0157272.
- Yang, H., Lv, Z., Wang, L., et al., 2023b. Stability mechanism of controlled acidresistant hydrophobic polymer nanospheres on CO₂ foam. Fuel 346, 128332. https://doi.org/10.1016/j.fuel.2023.128332.
- Yang, Z., Li, X., Li, D., et al., 2019. New method based on CO₂-switchable wormlike micelles for controlling CO₂ breakthrough in a tight fractured oil reservoir. Energy Fuels 33 (6), 4806–4815. https://doi.org/10.1021/acs.energyfuels.9b00362.
- Zhang, X., Deng, J., Yang, K., et al., 2022. High-strength and self-degradable sodium alginate/polyacrylamide preformed particle gels for conformance control to enhance oil recovery. Petrol. Sci. 19 (6), 3149—3158. https://doi.org/10.1016/ j.petsci.2022.06.012.
- Zhao, M., Yan, R., Li, Y., et al., 2022. Study on the thickening behavior and

- mechanism of supercritical CO₂ by modified polysiloxane. Fuel 323, 124358. https://doi.org/10.1016/j.fuel.2022.124358.
- Zhou, B., Kang, W., Jiang, H., et al., 2022a. Preparation and crosslinking mechanism of delayed swelling double-crosslinking nano polymer gel microsphere for anti-CO₂ gas channeling. J. Petrol. Sci. Eng. 219, 111122. https://doi.org/10.1016/ j.petrol.2022.111122.
- Zhou, B., Kang, W., Yang, H., et al., 2022b. Study of the reinforced mechanism of fly ash on amphiphilic polymer gel. Petrol. Sci. 19 (5), 2175–2184. https://doi.org/

- 10.1016/j.petsci.2022.05.019.

 Zou, J., Yue, X., Zhang, J., et al., 2018. Self-assembled microspheres feasibility study for conformance control in high temperature and high salinity reservoirs. Arabian J. Geosci. 11 (9), 195. https://doi.org/10.1007/s12517-018-3544-0.

 Zou, J., Yue, X., Dong, J., et al., 2020. Applications of in situ polymerization microsphere with surfactant EOR in low-permeability and heterogeneous reservoirs. Arabian J. Geosci. 13 (2), 89. https://doi.org/10.1007/s12517-020-5084-7.